Geometric and Algebraic Constraints of Projected Concentric Circles and Their Applications to Camera Calibration

Jun-Sik Kim, *Student Member*, *IEEE*,
Pierre Gurdjos, and
In-So Kweon, *Member*, *IEEE*

Abstract—We investigate the projective properties of the feature consisting of two concentric circles. We demonstrate there exist geometric and algebraic constraints on its projection. We show how these constraints greatly simplify the recoveries of the affine and Euclidean structures of a 3D plane. As an application, we assess the performances of two camera calibration algorithms.

Index Terms—Imaging geometry, concentric circles, projective plane, circular points, camera calibration.

1 Introduction

THE issue of inferring metric properties about the camera and the scene from projections of conic features has been intensively investigated in the computer vision literature, e.g., regarding calibration or structure from/and motion problems [1], [11], [12], [14], [16]. Conic features are arguably popular for one main reason: treated as targets, they can be easily detected and robustly estimated e.g., using the method of [4]. Quadrics and conics play a central role in projective geometry [17], which, for its part, has revealed to be an essential theory in designing unified frameworks for solving problems. For instance, [16] elegantly uses properties of quadric pencils to reconstruct the 3D planes of noncoplanar ellipses, from known projection matrices. In fact, the importance of conics and, in particular, of circles, is quite clear in the case of a plane-based world. The important following results include projective properties which, if satisfied for some planar entities, also hold for the imaged entities under any homography. 1) The *affine structure (AS)* of a 3D plane is given by its vanishing line, i.e., its imaged line at infinity, whereas the line at infinity is in pole-polar relation [17, p. 119] with the center of any conic. 2) The *Euclidean structure (ES)* is given by the imaged circular points (ICPs), whereas the *circular points* are, by definition [8, pp. 52-53], two complex conjugate points at infinity, common to all circles, including the absolute conic [8, pp. 81-83]. As a direct result of 2), thanks to [21], the plane-based calibration problem can be stated as that of fitting the imaged absolute conic (IAC) to $N \geq 3$ ICP-pairs, providing a closed-form solution for the intrinsic parameters [19], [25].

In computer vision, circular features are widely used, in particular, for calibration purpose. On this matter, one might criticize calibration algorithms to not entirely profit from the underlying projective properties of such features. For instance, in [9], [20], the centers of projected circles are generally treated as the projected centers of these circles, which is improper under general perspective projection. In search of a closed-form solution, this introduces a bias, which is removed later using iterative techniques. From our previous work [13], we know that, by replacing a circle by a pair of concentric circles, the projected center can be recovered very accurately. In plane-based calibration [19], [25], the ICPs are extracted from world-to-image homographies, themselves estimated from point correspondences, using corners as features, *not* circular features. So, why not recover the ICPs directly, using circles instead of points? This idea is tackled in recent works [15], [23], [24] which describe so-called new calibration techniques. The term "new" probably refers to the way the ICPs are recovered since the calibration itself is strictly based on the same well-known algorithms as in [19], [25]. In [24], no less than three projected coplanar concentric circles of known radii are required to compute the ICPs. Whereas [15] is discussed later in this section, [23] is worth dwelling on: The ICP-pair can be identified among the two intersection point-pairs of two projected unknown (arbitrary) circles, by distinguishing the two "associated lines" spanned by these pairs. Unfortunately, no technical aspect is discussed; without any other consideration, the prerequisite is to find the complex roots of a quartic equation, which may cause numerical instability. Other conic feature-based calibration techniques have been reported: In [10], ellipse correspondences are used for a camera undergoing pure rotational motion. In [2], [5], [13], the aim is to recover simultaneously the intrinsic and extrinsic parameters (the focal length is the only unknown in [2], [5]). Even if [2] deals with two arbitrary circles, all three minimization criteria are similar, based on the pose estimation problem as stated in [12]. By assuming known radii, only [5] is able to describe a linear solution. On the whole, these general techniques lead to rather complicated algorithms, if not nonlinear.[1]

The basic idea of this work is to treat a pair of concentric circles, with *unknown* center and radii, as a new artificial visual feature. The novelty is to provide new insights about the geometric structures it naturally encodes and to deal with the technical aspects of their recoveries. An application to plane-based camera calibration is described in Section 3.2.

Our starting point is [13], in which it is shown that the AS of the 3D plane is recovered, by imposing a rank-1 constraint on the linear combination of the two projected circle matrices. Our contributions in this paper are multiple. First, we show that it is possible to recover the ES, in terms of ICPs, in a way similar to [13], by imposing a rank-2 constraint. In particular, this leads us to explain why concentric circles require a special treatment by operating in the dual projective plane. The foundation of our reasoning is the geometry of linear systems of concentric circle envelopes, called *ranges of concentric circles* [17, pp. 156-158], in which the AS and the ES of the plane are simply encoded by degenerate members. Within this framework, we are able to state a theorem that restricts the locus of the centers of projected concentric circles to a line through the horizon point and the projected center. We are convinced that existing techniques could profit from our compact and efficient algorithms (e.g., cf. Table I). For instance, in [15], where the calibration pattern is made up of a circle and a set of lines through its center, we point out that the circle and its center, if treated as rank-3 and rank-1 envelopes, respectively (cf. Section 2.2.1), determine a range of concentric circles. As a result, two steps of their algorithm, namely, the computation of the vanishing line and its intersection with the projected circle, are no longer required.

2 Properties of Concentric Circles

2.1 Projections of 3D Circles

Let $\widetilde{\mathbf{X}} = (X, Y, Z, 1)^\top$ be the 3D homogeneous coordinates of a world point and $\mathbf{x} = (u, v, 1)^\top$ be the 2D homogeneous coordinates of its projection in the image plane. Points $\widetilde{\mathbf{X}}$ and $\mathbf{x}$ are related by the projection equation:

1. Plane-based calibration has a linear formulation once the ES of the plane is recovered, so a standard algorithm is: 1) recover the ES, 2) compute the internal parameters, 3) determine the pose, 4) refine estimates if necessary.

- *J.-S. Kim and I.-S. Kweon are with the Department of Electrical Engineering and Computer Science, KAIST Daejeon, Korea. E-mail: jskim@rcv.kaist.ac.kr, iskweon@kaist.ac.kr.*
- *P. Gurdjos is with the INPT at the Institut de Recherche en Informatique de Toulouse (IRIT), Univ. P. Sabatier, 118 route de Narbonne, 31062 Toulouse, France. E-mail: Pierre.Gurdjos@irit.fr.*

Manuscript received 25 Jan. 2004; revised 3 Oct. 2004; accepted 6 Oct. 2004; published online 10 Feb. 2005.
Recommended for acceptance by L. Quan.
For information on obtaining reprints of this article, please send e-mail to: tpami@computer.org, and reference IEEECS Log Number TPAMI-0050-0104.

$$s\mathbf{x} = \mathtt{K}[\mathtt{R} \mid \mathbf{t}]\widetilde{\mathbf{X}}, \tag{1}$$

where $s \in \mathbb{R}\backslash\{0\}$; $\mathtt{R}$ and $\mathbf{t}$ are, respectively, the rotation matrix and translation vector relating the camera and world coordinate systems; $\mathtt{K}$ is the intrinsic calibration matrix of the form:

$$\mathtt{K} \triangleq \begin{bmatrix} \alpha_u & \gamma & u_0 \\ 0 & \alpha_v & v_0 \\ 0 & 0 & 1 \end{bmatrix},$$

where α_u, α_v represent the focal length in terms of pixel dimensions in the u, v direction, respectively, (u_0, v_0) are the principal point pixel coordinates, and γ is the skew factor.

Without loss of generality, we will assume that the world space is restricted to one plane Π, with equation $Z = 0$ with respect to the world coordinate system. The projection equation (1) then simplifies to:

$$s\mathbf{x} = \mathtt{K}[\mathbf{r}_1 \quad \mathbf{r}_2 \quad \mathbf{t}]\mathbf{X} \triangleq \mathtt{H}\mathbf{X}, \tag{2}$$

where $\mathbf{X} \triangleq (X, Y, 1)^\top$ and $\mathbf{r}_1$, $\mathbf{r}_2$ are the first two columns of $\mathtt{R}$. We will refer to $\mathtt{H}$ as the *world-to-image homography*.

In the world plane Π, the equation of a circle of radius ρ, centered at (X_0, Y_0), is of the form:

$$\mathbf{X}^\top \mathtt{Q}\mathbf{X} = 0, \quad \mathtt{Q} \triangleq \begin{bmatrix} 1 & 0 & -X_0 \\ 0 & 1 & -Y_0 \\ -X_0 & -Y_0 & X_0^2 + Y_0^2 - \rho^2 \end{bmatrix}, \tag{3}$$

while, in the image plane, points of the projected circle satisfy the conic equation:

$$\mathbf{x}^\top \mathtt{A}\mathbf{x} = 0, \quad \lambda\mathtt{A} \triangleq \mathtt{H}^{-\top}\mathtt{Q}\mathtt{H}^{-1}, \tag{4}$$

for $\lambda \in \mathbb{R}\backslash\{0\}$. We will refer to $\mathtt{Q}$ and $\mathtt{A}$ as the circle and projected circle, and to $\mathtt{Q}^{-1}$ and $\mathtt{A}^{-1}$ as the circle and projected circle envelopes,[2] respectively.

The center of $\mathtt{Q}$ is, by definition [17, p. 119], the pole of the line at infinity $\mathbf{L}_\infty \triangleq (0, 0, 1)^\top$ with respect to $\mathtt{Q}^{-1}$, i.e., $(X_0, Y_0, 1)^\top \sim \mathtt{Q}^{-1}\mathbf{L}_\infty$. In the image, the projected center is the pole of the vanishing line $\mathbf{v} \triangleq \mathtt{H}^{-\top}(0, 0, 1)^\top$ with respect to $\mathtt{A}^{-1}$, i.e., $\mathtt{H}(X_0, Y_0, 1)^\top \sim \mathtt{A}^{-1}\mathbf{v}$. In other words, the projected center, associated with $\mathtt{A}$, also specifies the AS of Π.

2.2 Algebraic Constraints: Rank Deficiency

According to (4), two concentric circles $\mathtt{Q}_j$ ($j \in \{1, 2\}$), project under $\mathtt{H}$ to conics $\mathtt{A}_j$ satisfying:

$$\lambda_j \mathtt{A}_j = \mathtt{H}^{-\top}\mathtt{Q}_j\mathtt{H}^{-1}. \tag{5}$$

Dually, the circle envelope $\mathtt{Q}_j^{-1}$ projects to the conic envelope:

$$(1/\lambda_j)\mathtt{A}_j^{-1} = \mathtt{H}\mathtt{Q}_j^{-1}\mathtt{H}^\top. \tag{6}$$

We assume that the circles are centered at the origin. Thus, referring to (3), $\mathtt{Q}_j$ and $\mathtt{Q}_j^{-1}$ are simply the diagonal matrices:

$$\mathtt{Q}_j = \mathrm{diag}(1, 1, -\rho_j^2) \quad \text{and} \quad \mathtt{Q}_j^{-1} = \mathrm{diag}(1, 1, -1/\rho_j^2).$$

Now, let us consider a linear combination of the form:

$$\Delta \triangleq \alpha_1 \mathtt{A}_1^{-1} - \alpha_2 \mathtt{A}_2^{-1} \quad \text{satisfying} \quad \det \Delta = 0, \tag{7}$$

for some α_1, $\alpha_2 \in \mathbb{R}\backslash\{0\}$. The constraint in (7) is a degree-3 polynomial equation in $\beta \triangleq \alpha_1/\alpha_2$ with real factors, whose real roots are also those of:

$$\det(\beta\mathtt{Q}_1^{-1} - \lambda_2/\lambda_1\mathtt{Q}_2^{-1}) = 0. \tag{8}$$

2. As a conic is the assemblage of its points, a conic envelope is the assemblage of its (tangent) lines.

With no difficulty, it can be shown that these roots are:

$$\beta_1 = \lambda_2/\lambda_1 \text{ (with multiplicity 2)}, \quad \beta_2 = \lambda_2/\lambda_1(\rho_1/\rho_2)^2. \tag{9}$$

Since it is singular, Δ is the matrix of a degenerate conic envelope which consists of either two points or a repeated point [17, pp. 117-118]. As there is a double root, there are only two Δ as defined in (7), which are those determined by β_1, β_2 in (9). Let us find out what are these two associated degenerate conics by analyzing their matrices.

2.2.1 Rank-1 Constraint and AS

If we substitute α_1/α_2 for β_1 in (7), we get the rank-1 matrix:

$$\Delta_1 \triangleq \beta_1 \mathtt{A}_1^{-1} - \mathtt{A}_2^{-1} \sim \mathtt{H}\,\mathrm{diag}(0, 0, 1)\mathtt{H}^\top = \mathbf{c}\mathbf{c}^\top, \tag{10}$$

where $\mathbf{c} \triangleq \mathtt{H}(0, 0, 1)^\top$.

The center of the concentric circles coincides with the origin of Π, so it is clear that $\mathbf{c}$ is its projection. Hence, Δ_1 can be seen as the degenerate conic envelope consisting of the projected center taken twice, that we call the projected *conic dual to the circle center* (CDCC).

Note that, since $\mathbf{c}$ is the pole of the vanishing line, with respect to $\mathtt{A}_1^{-1}$ and $\mathtt{A}_2^{-1}$, the projected CDCC Δ_1 encodes the AS of Π.

2.2.2 Rank-2 Constraint and ES

If we substitute α_1/α_2 for β_2 in (7), we get the rank-2 matrix:

$$\Delta_2 \triangleq \beta_2 \mathtt{A}_1^{-1} - \mathtt{A}_2^{-1} \sim \mathtt{H}\,\mathrm{diag}(1, 1, 0)\mathtt{H}^\top. \tag{11}$$

Using (6), we note that Δ_2 is the projection of the rank-2 conic envelope $\mathtt{C}_\infty^* \triangleq \mathrm{diag}(1, 1, 0)$ of Π. It can easily be stated that $\mathtt{C}_\infty^*$ consists of the two circular points $\mathbf{I} \triangleq (1, i, 0)^\top$, $\mathbf{J} \triangleq (1, -i, 0)^\top$, $i^2 = -1$, on $\mathbf{L}_\infty$, i.e.,

$$\mathtt{C}_\infty^* \sim \mathbf{I}\mathbf{J}^\top + \mathbf{J}\mathbf{I}^\top.$$

$\mathtt{C}_\infty^*$ is known as the *conic dual to the circular points* (CDCP) [8, pp. 53-56]. As an important result, Δ_2 encodes the ES of Π. It is worth mentioning that the ICPs are in the form of $\mathbf{x}_1 \pm i\mathbf{x}_2$, where $\mathbf{x}_1, \mathbf{x}_2$ are the first two columns of $\mathtt{X} \in \mathbb{R}^{3\times3}$ resulting from the singular value decomposition (SVD) of Δ_2, providing it is written as $\Delta_2 = \mathtt{X}\,\mathrm{diag}(1, 1, 0)\mathtt{X}^\top$. The only line of Δ_2 that contains both ICPs is the vanishing line $\mathbf{v}$, so $\Delta_2\mathbf{v} = 0$, i.e., $\mathbf{v}$ spans the null space of Δ_2.

2.3 Geometric Constraint: Locus of Centers of Projected Circles

The algebraic constraints about rank deficiency, established in Section 2.2, can be interpreted in terms of the projective geometry of a range of concentric circles [17, pp. 156-158], i.e., a (simply infinite) linear system of concentric circle envelopes, that includes the CDCC and CDCP as degenerate members, as illustrated in Fig. 1. A pure geometric constraint, by means of a theorem, will be now inferred using this framework but, first, we have to state some preliminary results.

Call *pole of a line* $\mathbf{L}$ *with respect to the CDCP* $\mathtt{C}_\infty^*$ the point at infinity $\mathtt{C}_\infty^*\mathbf{L}$ which is the direction of all parallel lines perpendicular to $\mathbf{L}$. The pole of the projected line $\mathbf{l} = \mathtt{H}^{-\top}\mathbf{L}$ with respect to the projected CDCP Δ_2 is the vanishing point $\Delta_2\mathbf{l} = \mathtt{H}\mathtt{C}_\infty^*\mathbf{L}$.

Define the *horizon point* $\mathbf{p}_\mathbf{v}$ as the point intersecting the vanishing line $\mathbf{v}$ and the line, perpendicular to $\mathbf{v}$ and containing the principal point, called *principal line* [7],[3] cf. Fig. 2. The principal line is in the *principal plane*, containing the camera center and perpendicular to the intersection $(\Pi \cap \mathcal{F})$ of Π and the focal plane[4] $\mathcal{F}$. Albeit little-mentioned in computer vision textbooks, these are familiar notions in photogrammetry [18, pp. 41-42] and considered as orientation elements.

3. To avoid confusion with the center of a circle, we rename the *center line and plane* of [7], as *principal line and plane*, in accordance with [18].

4. Containing the camera center and parallel to the image plane [3, p. 35].

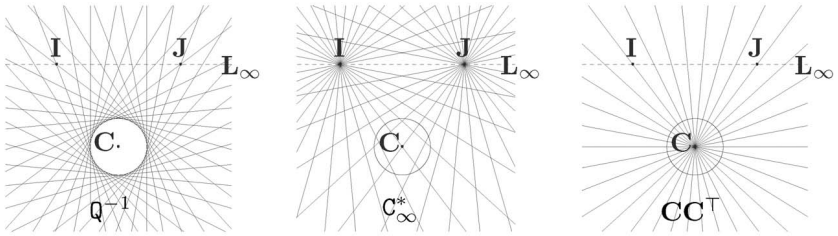

Fig. 1. (a) The (rank-3) circle envelope $\mathtt{Q}^{-1}$. (b) The (rank-2) envelope $\mathtt{C}^*_\infty$, consisting of the circular points $\mathbf{I}, \mathbf{J}$ (on the line at infinity $\mathbf{L}_\infty$). (c) The (rank-1) envelope $\mathbf{CC}^\top$, consisting of the circle center $\mathbf{C}$ (taken twice). Conics (b) and (c) are degenerate members of the range of circles centered at $\mathbf{C}$.

Lemma 1. *The horizon point $\mathbf{p_v}$ is the pole of the image plane's line at infinity $\mathbf{l}_\infty$ with respect to the projected CDCP Δ_2; its vector is the third column of Δ_2.*

Proof. We want to show that $\mathbf{p_v} \sim \Delta_2 \mathbf{l}_\infty$ in the image, i.e., $\mathtt{H}^{-1}\mathbf{p_v} \sim \mathtt{C}^*_\infty \mathtt{H}^\top \mathbf{l}_\infty$ in Π. In other words, since $\mathtt{H}^\top \mathbf{l}_\infty$ is the preimage of $\mathbf{l}_\infty$, that is the line $(\Pi \cap \mathcal{F})$, it suffices to show this point: Any line with direction $\mathtt{H}^{-1}\mathbf{p_v}$ in Π (they are all parallel) is perpendicular to $(\Pi \cap \mathcal{F})$. The principal line contains $\mathbf{p_v}$ so its preimage in Π is a candidate. By definition, the principal plane is perpendicular to $(\Pi \cap \mathcal{F})$. Since it contains the principal line and its preimage, this point holds. The fact that $\mathbf{l}_\infty = (0,0,1)^\top$ completes the proof. □

Note that, we implicitly excluded that $\mathtt{H}$ is a 2D affinity[5] or else $\Delta_2 \mathbf{l}_\infty = \mathbf{0}$; the horizon point would not be defined.

Theorem 1. *In the world plane, let $\mathtt{Q}_j$ denote a variable circle concentric with a fixed circle $\mathtt{Q}$. The locus $\mathcal{L}$ of the center of the projection of $\mathtt{Q}_j$ is a point or a line through the projected center of $\mathtt{Q}$ and the horizon point; the only degree of freedom of the center with respect to this line is the radius of $\mathtt{Q}_j$.*

Proof. Define the line at infinity $\mathbf{l}_\infty \triangleq (0,0,1)^\top$. Let $\mathtt{A}$, $\mathtt{A}_j$ denote the projections of $\mathtt{Q}$, $\mathtt{Q}_j$, according to (5). Since it is common to all $\mathtt{Q}_j$, let us call the center $\mathbf{C}$ of $\mathtt{Q}$ the *defining center*. As an immediate result of (10), we have:

$$\Delta_1 \mathbf{l}_\infty = \beta_1 \mathtt{A}^{-1}\mathbf{l}_\infty - \mathtt{A}_j^{-1}\mathbf{l}_\infty \triangleq s\mathbf{c}, \tag{12}$$

where $s \in \mathbb{R}\backslash\{0\}$. This means that the projection $\mathbf{c}$ of the defining center $\mathbf{C}$ is on the line $\mathcal{L}$ spanned by the two centers of the projected circles, which are the poles of $\mathbf{l}_\infty$ with respect to $\mathtt{A}^{-1}$ and $\mathtt{A}_j^{-1}$. Similarly, as an immediate result of (11), we have:

$$\Delta_2 \mathbf{l}_\infty = \beta_2 \mathtt{A}^{-1}\mathbf{l}_\infty - \mathtt{A}_j^{-1}\mathbf{l}_\infty \triangleq \boldsymbol{\phi}. \tag{13}$$

Thanks to the lemma, this means that, providing $\boldsymbol{\phi} \neq \mathbf{0}$, $\boldsymbol{\phi}$ is the horizon point and is also on $\mathcal{L}$. Now, subtract (12) from (13) in order to eliminate $\mathtt{A}^{-1}\mathbf{l}_\infty$. As a result, there necessarily exist a_1, $a_2 \in \mathbb{R} \setminus \{0\}$ such that:

$$\mathtt{A}_j^{-1}\mathbf{l}_\infty = a_1\mathbf{c} + a_2\boldsymbol{\phi}. \tag{14}$$

First, consider the case where the horizon point is not defined, i.e., $\boldsymbol{\phi} = \mathbf{0}$. This happens if and only if $\mathbf{l}_\infty \sim \mathbf{v}$, i.e., $\mathtt{H}$ is a 2D affinity (the world plane is then parallel to the image plane).

It follows that $\mathtt{A}_j^{-1}\mathbf{l}_\infty \sim \mathbf{c}$; hence, the center of $\mathtt{A}_j$ coincides with the projected center of $\mathtt{Q}_j$. In other cases, (14) tells us that the center of the projected circle number j is on the line $\mathcal{L}$, passing through the projected defining center and the horizon point. Finally, note that, using (6), we get:

$$\mathtt{A}_j^{-1}\mathbf{l}_\infty = \mathtt{H}\,\mathrm{diag}(1,1,-1/\rho_j^2)(H_{31}, H_{32}, H_{33})^\top, \tag{15}$$

so the center of the projected circle number j is the projection of a point controlled by its radius ρ_j, with pixel inhomogeneous coordinates $-\rho_j^2(H_{31}/H_{33}, H_{32}/H_{33})$ in Π. □

Two remarks can be made. On the one hand, the advised reader will note that the theorem could have been formulated in a more general way since *the locus of poles of a line with respect to a range of concentric circles is a second line*, as established in [17, pp. 168-169]. Regarding our problem, this had to be considered in the special case of $\mathbf{l}_\infty$. On the other hand, the locus of centers of multiple pairs of projected concentric circles is a linear system of lines, whose vertex (i.e., common point) is the horizon point. This pencil has for preimage in the world plane Π a set of all (parallel) lines perpendicular to $(\Pi \cap \mathcal{F})$, cf. Fig. 2.

Whatever the recovery is about, either the projected center or the ICPs, the issue to be tackled next is how to determine β_1 and β_2 that solve (8), while keeping in mind that β_1 is a double root. In practice, using result (9) is not possible since the ratio of scale factors λ_2/λ_1 is unknown and the ratio of radii ρ_1/ρ_2 is not always given. There are various ways to determine β_1 and β_2, without knowing λ_2/λ_1 and ρ_1/ρ_2. One can compute them as the generalized eigenvalues [6, p. 375] of the pair $\{\mathtt{A}_1, \mathtt{A}_2\}$ or, equivalently, as the eigenvalues of $\mathtt{A}_1\mathtt{A}_2^{-1}$, or simply by solving the cubic equation (8). Since β_1 is a root of multiplicity two, it suffices to distinguish it from β_2 (for instance, refer to the MATLAB code given in Table 1).

Thanks to our theorem, there is an alternate way of computing $\mathbf{c}$. Denoting by $\mathbf{a}_j$, $\mathbf{b}_j$ the two points at which $\mathcal{L}$ meets[6] the projected circle $\mathtt{A}_j$ (cf. Fig. 3), it is based on the harmonic relation [17, p. 48] between the two pairs of collinear points $\{\mathbf{a}_j, \mathbf{b}_j\}$ and $\{\mathbf{c}, \boldsymbol{\phi}\}$, i.e., the invariance of cross ratios:

$$\mathrm{cross}(\mathbf{a}_j, \mathbf{b}_j; \mathbf{c}, \boldsymbol{\phi}) = \mathrm{cross}(\mathbf{A}_j, \mathbf{B}_j; \mathbf{C}, \boldsymbol{\Phi}_\infty) = -1, \tag{16}$$

where $\mathbf{A}$, $\mathbf{B}$, $\mathbf{C}$, $\boldsymbol{\Phi}_\infty$ are the respective preimages of $\mathbf{a}$, $\mathbf{b}$, $\mathbf{c}$, $\boldsymbol{\phi}$ in the world plane ($\boldsymbol{\Phi}_\infty$ is at infinity). Given $j \in \{1,2\}$, we obtain a unique solution for $\mathbf{c}$ such that $\mathbf{c}$ is on both segments $(\mathbf{a}_j, \mathbf{b}_j)$. Fig. 3 shows the estimated projected center using this geometric property.

3 Application: Camera Calibration

3.1 Recovering the Projected Circular Points

On the basis of the constraints described in Sections 2.2 and 2.3, we design two algorithms for recovering the ES of the world plane, i.e., its ICPs, from a single view.

The first (ALG-CDCP) is a direct application of the rank-2 constraint given in Section 2.2.2, it recovers the projected CDCP from the pair of projected concentric circles $\{\mathtt{A}_1, \mathtt{A}_2\}$.

- Given $\{\mathtt{A}_1, \mathtt{A}_2\}$, compute Δ_2 from the rank-2 constraint described in (11).

5. Such that the third row of $\mathtt{H}$ is $(0,0,1)$ and the third column of Δ_2 is $\mathbf{0}$.

6. There exists a very elegant way of finding $\mathbf{a}_j$ and $\mathbf{b}_j$ by solving a Joachimsthal equation [17, p. 107].

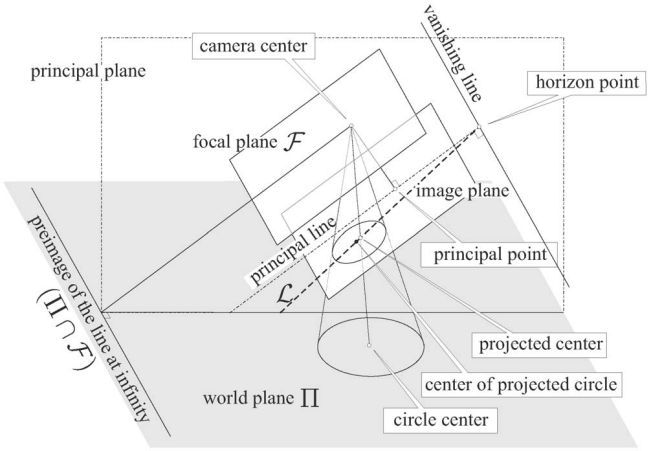

Fig. 2. The locus of the center of the projection of a variable circle, having a fixed center (and, so, a varying radius), is a line $\mathcal{L}$ (shown in dashed) through the horizon point and the projected center of the circle.

- Recover the ICPs in the form of $\sqrt{s_1}\mathbf{u}_1 \pm i\sqrt{s_2}\mathbf{u}_2$, where $\mathbf{u}_1$ and $\mathbf{u}_2$ are the first two columns of U resulting from the SVD $\Delta_2 = \mathtt{U}\,\mathrm{diag}(s_1, s_2, 0)\mathtt{U}^\top$; $\mathtt{U}\mathtt{U}^\top = \mathrm{I}$.

Table 1 illustrates the compactness of the implementation of this algorithm in MATLAB.

The second (ALG-CC) recovers the ICPs from $P \geq 4$ pairs of projected concentric circles. It is assumed that the circle centers have known Euclidean coordinates in the world plane Π, with no degenerate configuration.

- Given $\{\mathtt{A}_{1p}, \mathtt{A}_{2p}\}$, $p \in \{1, .., P\}$, compute the projected center $\mathbf{c}_p$ by solving (16).
- Compute the world-to-image homography H, e.g., using the normalized DLT algorithm, as detailed in [8, p. 109].
- Recover the ICPs in the form of $\mathbf{h}_1 \pm i\mathbf{h}_2$, where $\mathbf{h}_1$ and $\mathbf{h}_2$ are the first two columns of H.

Regarding ALG-CC, from Sections 2.2 and 2.3, we actually have at our disposal several ways of determining $\mathbf{c}_p$; the choice of the method here is somewhat arbitrary since, practically, all of these yield highly similar results.

3.2 Computing the Internal Parameters

Like there is an Euclidean specialization of the (dual) projective plane once the CDCP is identified, there is an Euclidean specialization of the (dual) projective 3D space, once the dual absolute quadric (DAQ) [8, pp. 462-463] is identified. The DAQ projects to the dual IAC, whose matrix $\boldsymbol{\omega}^*$ encodes the intrinsic properties of the camera, via the Cholesky factorization $\boldsymbol{\omega}^* = \mathtt{K}\mathtt{K}^\top$ involving the calibration matrix K. For some practical reasons, the plane-based calibration of the camera, i.e., the determination of K, is performed in the regular plane, by estimating the IAC $\boldsymbol{\omega} \sim (\boldsymbol{\omega}^*)^{-1}$ as the locus of all ICPs, through a linear formulation of the problem [19], [21], [25]. Each view contributes two equations linear in the elements of the unknown 6-vector $\mathbf{x}$, $\|\mathbf{x}\|^2 = 1$, corresponding to the upper diagonal of $\boldsymbol{\omega}$; so, providing K is constant, three views are necessary to obtain a solution.

Since plane-based calibration and its implementation has been widely outlined in [19], [25], we will not give more details here; Let us just mention the exhaustive study of degenerate configurations in [19].

TABLE 1
Computing the ICPs from Matrices A1, A2 of Projected Concentric Circles in Four MATLAB Instructions

```
e = eig(A1, A2);
[m, k] = max(abs(median(e)-e));
[U, S, V] = svds(e(k)*inv(A1)-inv(A2), 2);
ICP = U*sqrt(S)*[1;±i]; % i^2=-1
```

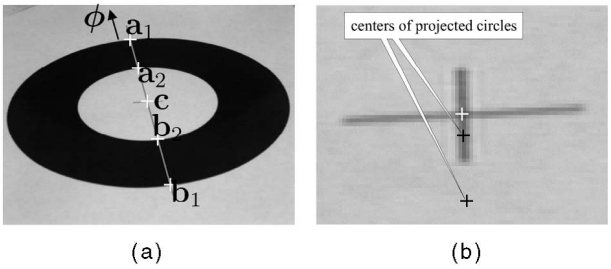

Fig. 3. (a) Projected circles and line $\mathcal{L}$ of centers of projected circles. (b) Centers of projected circles (black crosses) and estimated circle projected center (white cross) using the method given in Section 2.3.

4 Experiments

4.1 Synthetic Data

Experiments are conducted using synthetic data to assess the performances of our algorithms in presence of noise. The scene consists of a planar patch, with size $500\mathrm{mm} \times 500\mathrm{mm}$, called $1\text{-}pattern$ or $n \times n\text{-}pattern$, depending on whether it is covered with a single pair or n^2 equally spaced identical pairs of concentric circles. The camera is at a distance of $1,800\mathrm{mm}$. The inclination angle between world and image planes, as well as the angles of azimuth and rotation around the optical axis, vary within the range $[-60°; 60°]$. The simulated camera has a 512×512 pixel resolution and constant internal parameters $u_0 = 255$, $v_0 = 255$, $\alpha_u = 1,200$, $\alpha_u = 1,080$, and $\gamma = 0$. Each circle of the pattern projects to an ellipse, which is digitized at pixel resolution, yielding S sampled pixels. Gaussian noise of zero mean and standard deviation σ is added to the pixel (integer) coordinates. The tests in the following Sections 4.1.1 and 4.1.2 are repeated 500 times each.

4.1.1 Estimation of the Projected Centers

Using kS randomly selected points per ellipse, $k \in \{0.25, .., 1\}$, we investigate the influence of simulation parameters in determining the projected center, by solving (16). We conduct a first series of three tests, by computing and plotting the average distances between true and estimated projected centers. Results are shown in Fig. 5, where the numbers of sampled points for the inner ellipses are plotted vertically. In tests (a) and (b), we deal with a 1-pattern. For $\sigma = 1$, Fig. 5a shows the influence of the radius ratio $r \in \{0.1, .., 0.9\}$. For $r = 0.5$, Fig. 5b shows the influence of $\sigma \in \{0, .., 3\}$. In Fig. 5c, we deal with a $n \times n\text{-pattern}$, $n \in \{1, .., 7\}$. For $\sigma = 1$ and $r = 0.5$, it shows how the error varies if we replace the 1-pattern by a $n \times n\text{-pattern}$ (i.e., with smaller radii), by computing the average error for the n^2 pairs. These results highlight a number of interesting characteristics. The "ideal" radius ratio seems to be around 0.5, while degeneracies predictably occur when it tends to 1. Using a 1-pattern,

Fig. 4. Examples of generated occluding images.

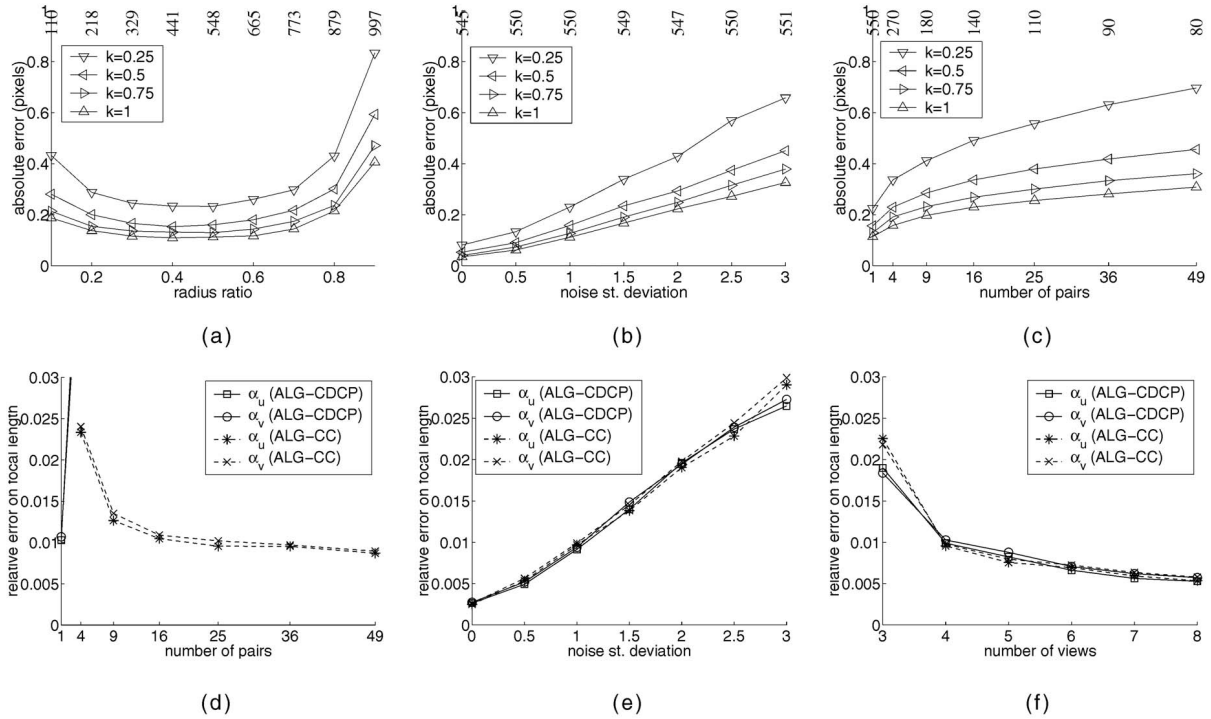

Fig. 5. (a), (b), and (c) Errors on the estimated projected centers, depending on the number of sampled points (i.e., for a varying coefficient k). The number of points ($k = 1$) for the inner projected circle is plotted vertically. (d), (e), and (f) Errors on the estimated focal lengths obtained by the proposed algorithms, using four views.

we can reasonably expect to estimate the projected center with a precision of ≈ 0.2 pixel, up to $\sigma = 2$. At the other extreme, i.e., using a 7×7-pattern, the precision is ≈ 0.4 pixels for $\sigma = 1$, even if it is worth noting that, in Fig. 5c, the increase of the error function is at a peak when changing from a 1-pattern to a 2×2-pattern.

4.1.2 Plane-Based Calibration

In the second series of three tests, we assess the performance of camera calibration, using the algorithm of Section 3.2, taking as input the ICPs computed by ALG-CDCP and ALG-CC, as detailed in Section 3.1 (cf. Table 1 for ALG-CDCP's implementation). We investigate the influence of simulation parameters in estimating the focal length in terms of α_u and α_v. All these tests are carried out with radius ratio $r = 0.5$; the number of views is 4, except in Fig. 5f. In Fig. 5d, for $\sigma = 1$, it is shown how the error varies if we replace the 1-pattern by a $n \times n$-pattern. For ALG-CDCP, n^2 ICP-pairs are computed, although they are all identical in absence of noise. In tests (e) and (f), we use a 1-pattern for ALG-CDCP and a 5×5-pattern for ALG-CC. Fig. 5e shows the influence of $\sigma \in \{0, .., 3\}$. Fig. 5f shows the influence of the number of views. The main characteristic of this series is that calibration performs similarly using ALG-CDCP with a 1-pattern, or ALG-CDCP with a 5×5-pattern. Note that ALG-CC can be seen as the conventional approach of [19], [25], with circle centers as feature points, with one difference: The standard deviation ($\sigma = 1$) of noise perturbing image points is four times the average error (≈ 0.25) on the estimated projected centers.

4.2 Real Data

To test the performance with respect to the partial viewing condition caused by occlusion or field of view (FOV) limitation, we calibrated cameras under various occluding conditions. Fig. 4 shows some images of concentric circle patterns with intentional occlusions. The images were captured using a SONY F-828 (640×480) camera. After edge detection using Canny operator [3, pp. 98-101], projected circle fitting and IAC fitting were achieved by direct least square fitting of ellipses as implemented by Fitzgibbon et al. [4]. Tsai's calibration method [22] has been used to obtain the ground truth data. Table 2 shows the error of the estimated parameters under various occlusion conditions. Even though the occlusion rate increases up to almost 50 percent, the calibration has been accomplished robustly. To show the practicality of the proposed algorithm, we applied it to multi-camera calibration, using 10 SONY DFW-V500 cameras, for the reconstruction of a 3D scene. In this case, the captured images suffer from FOV limitation. Table 3 shows an example of edge processing and the calibration matrix estimated by our algorithm.

5 Conclusion

We suggested to treat a pair of projected concentric circles, with unknown center and radii, as a new artificial visual feature. As shown throughout the paper, this is motivated by the fact that such a feature naturally encloses the affine and Euclidean structures of the supporting 3D plane. These entities are given point-wise in terms of the circle projected (common center) and projected circular points, respectively. Geometrically speaking, we operate in the dual projective plane, by studying the degenerate members of the linear system of conic envelopes, whose basis are the two projected concentric circle envelopes. Algebraically, it requires to seek some linear combinations of the matrices of the base conics that are

TABLE 2
Relative Error on Focal Length with Respect to Various Occlusion Rates

Situation	Error in α_u	Error in α_v
No occlusion	0.002	0.016
26% occlusion	0.014	0.002
30% occlusion	0.006	0.022
47% occlusion	0.020	0.002

TABLE 3
Input Images, Edge Map, and the Estimated Calibration Matrix

Input images	Edge map	Resulting matrix
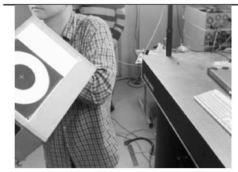		$\begin{bmatrix} 846.8486 & -20.6596 & 334.6779 \\ 0 & 834.6534 & 226.8914 \\ 0 & 0 & 1.0000 \end{bmatrix}$

rank-deficient. We shown there exist compact and efficient algorithms that compute very accurate solutions (e.g., cf. Table 1). Moreover, we described a geometric constraint that restricts the locus of centers of projected concentric circles to a line through the projected center and the horizon point on the vanishing line, this latter being irrespective of the projected circles. Regarding potential applications, the results of our algorithms can be used as data in plane-based camera calibration [19], [25]. The fact that the geometric structures of the 3D plane are described by rank-deficient matrices greatly simplifies the calibration algorithm. Algorithms have been tested with both synthetic data sets and real images. Our conic-based approach shows the superior performance to the conventional point-based ones. It makes the calibration robust even with partial viewing condition due to occlusion or FOV limitation.

ACKNOWLEDGMENTS

This research has been supported by the Korean Ministry of Science and Technology for National Research Laboratory Program (Grant number M1-0302-00-0064) and by a collaboration between RRV-KAIST in Korea and TCI-IRIT in France.

REFERENCES

[1] S. Avidan and A. Shashua, "Trajectory Triangulation: 3D Reconstruction of Moving Points from a Monocular Image Sequence," *IEEE Trans. Pattern Analysis and Machine Intelligence,* vol. 22, no. 4, pp. 348-357, Apr. 2000.
[2] Q. Chen, H. Wu, and T. Wada, "Camera Calibration with Two Arbitrary Coplanar Circles," *Proc. European Conf. Computer Vision,* vol. 3, pp. 521-532, 2004.
[3] O. Faugeras, *Three-Dimensional Computer Vision.* MIT Press, 1993.
[4] A. Fitzgibbon, M. Pilu, and R.B. Fisher, "Direct Least Square Fitting of Ellipses," *IEEE Trans. Pattern Analysis and Machine Intelligence,* vol. 21, no. 5, pp. 476-480, May 1999.
[5] V. Frémont and R. Chellali, "Direct Camera Calibration Using Two Concentric Circles from a Single View," *Proc. Int'l Conf. Artificial Reality and Telexistence,* pp. 93-98, 2002.
[6] G. Golub and C. Van Loan, *Matrix Computation,* third ed. Johns Hopkins Univ. Press, 1996.
[7] P. Gurdjos, A. Crouzil, and R. Payrissat, "Another Way of Looking at Plane-Based Calibration: The Centre Circle Constraint," *Proc. European Conf. Computer Vision,* vol. 4, pp. 252-266, 2002.
[8] R. Hartley and A. Zisserman, *Multiple View Geometry in Computer Vision,* second ed. Cambridge Univ. Press, 2003.
[9] J. Heikkila, "Geometric Camera Calibration Using Circular Control Points," *IEEE Trans. Pattern Analysis and Machine Intelligence,* vol. 22, no. 10, pp. 1066-1077, Oct. 2000.
[10] R. Hu and Q. Ji, "Camera Self-Calibration from Ellipse Correspondences," *Proc. IEEE Int'l Conf. Robotics and Automation,* vol. 3, pp. 2191-2196, 2001.
[11] G. Jiang, H.-T. Tsui, and L. Quan, "Circular Motion Geometry Using Minimal Data," *IEEE Trans. Pattern Analysis and Machine Intelligence,* vol. 26, no. 6, pp. 721-731, June 2004.
[12] K. Kanatani and W. Liu, "3D Interpretation of Conics and Orthogonality," *Computer Vision and Image Understanding,* vol. 58, no. 3, pp. 286-301, Nov. 1993.
[13] J.-S. Kim, H.-W. Kim, and I.-S. Kweon, "A Camera Calibration Method Using Concentric Circles for Vision Applications," *Proc. Asian Conf. Computer Vision,* vol. 2, pp. 515-520, 2002.
[14] S.D. Ma, "Conics-Based Stereo, Motion Estimation, and Pose Determination," *Int'l J. Computer Vision,* vol. 10, no. 1, pp. 7-25, Feb. 1993.
[15] X. Meng and Z. Hu, "A New Easy Camera Calibration Technique Based on Circular Points," *Pattern Recognition,* vol. 36, no. 5, pp. 1155-1164, May 2003.
[16] L. Quan, "Conic Reconstruction and Correspondence from Two Views," *IEEE Trans. Pattern Analysis and Machine Intelligence,* vol. 18, no. 2, pp. 151-160, Feb. 1996.
[17] J. Semple and G. Kneebone, *Algebraic Projective Geometry.* Oxford Classic Series, Clarendon Press, 1952, reprinted, 1998.
[18] C.C. Slama, *Manual of Photogrammetry,* fourth ed. Am. Soc. Photogrammetry, 1980.
[19] P. Sturm and S. Maybank, "On Plane-Based Camera Calibration: A General Algorithm, Singularities, Applications," *Proc. IEEE Conf. Computer Vision and Pattern Recognition,* vol. 1, pp. 432-437, 1999.
[20] J.-P. Tarel and A. Gagalowicz, "Calibration de Caméra à Base d'Ellipses," *Traitement du Signal,* vol. 12, no. 2, pp. 177-187, 1995.
[21] B. Triggs, "Autocalibration from Planar Scenes," *Proc. European Conf. Computer Vision,* vol. 1, pp. 89-105, 1998.
[22] R. Tsai, "A Versatile Camera Calibration Technique for High Accuracy 3D Machine Vision Metrology Using Off-The-Shelf TV Cameras and Lenses," *IEEE J. Robotics and Automation,* vol. 3, no. 4, pp. 323-344, Aug. 1987.
[23] Y. Wu, H. Zhu, Z. Hu, and F. Wu, "Camera Calibration from Quasi-Affine Invariance of Two Parallel Circles," *Proc. European Conf. Computer Vision,* vol. 1, pp. 190-202, 2004.
[24] C. Yang, F. Sun, and Z. Hu, "Planar Conic Based Camera Calibration," *Proc. Int'l Conf. Pattern Recognition,* vol. 1, pp. 555-558, 2000.
[25] Z. Zhang, "A Flexible New Technique for Camera Calibration," *IEEE Trans. Pattern Analysis and Machine Intelligence,* vol. 22, no. 11, pp. 1330-1344, Nov. 2000.